TECHNICAL PAPER





Studies on Corrosion of Titanium and Air-Oxidized Titanium in Fluorinated Nitric Acid

J. Jayaraj¹ P. M. Ranjith² S. Ningshen¹ S. Ramanathan²

Received: 28 November 2018/Accepted: 18 March 2019/Published online: 6 April 2019 © The Author(s) 2019

Abstract Titanium (Ti) is a lustrous transition metal which possesses excellent corrosion resistance in several aggressive environments but is attacked by acidic fluoride media. In this work, the addition of fluoride ion to nitric acid on the corrosion behavior of Ti and air-oxidized Ti was studied. Air oxidation of Ti at 800 °C for 5 h resulted in the formation of an intact rutile TiO2 layer with a thickness of about 35 µm. The corrosion resistance was investigated from the polarization resistance (R_P) values which were obtained from linear polarization and electrochemical impedance spectroscopy (EIS) measurements. A decrease in the R_P value of Ti with the addition of fluoride ion in nitric acid was observed, and this indicated the formation of an unstable layer, which resulted in accelerated dissolution. The several order increase in the R_P value of air-oxidized Ti in nitric acid containing fluoride ions pointed the improved resistance to corrosion. The diffusivity of species through the air-oxidized TiO₂ layer was estimated from the electrochemical equivalent circuit (EEC) analysis of EIS data. Even though the diffusivity

increased by several orders with the addition of fluoride ions, air-oxidized Ti provided better protection against nitric acid containing fluoride ions than Ti. The corrosion rates of Ti and air-oxidized Ti in boiling nitric acid containing fluoride ions were also estimated from weight loss experiments. Even in boiling fluorinated nitric acid, air-oxidized Ti provided better corrosion protection, with corrosion rates of about 1000 times less than that of Ti.

Keywords Titanium · Air oxidation · Linear polarization · EIS · Weight loss measurement · Fluorinated nitric acid

1 Introduction

The compact reprocessing of advanced fuels in leadshielded cell (CORAL) facility at India utilizes commercially pure titanium grade 2 as dissolver vessel for the dissolution of spent mixed carbide fuels in boiling 11.5 M nitric acid [1]. In contrast, Zirconium 702 is used as the dissolver and evaporator units of the La-Hague reprocessing plant, France [2]. Boiling 11.5 M HNO₃ + 0.05 MNaF was proposed for the dissolution of spent mixed oxide $(72\%UO_2 - 28\%PuO_2)$ fuels, [3] and the addition of fluoride ions is highly necessary for its complete dissolution [4]. However, zirconium and titanium exhibited high corrosion resistance in boiling nitric acid, but showed poor corrosion in nitric acid containing fluoride ions [3, 5]. It was confirmed that the corrosion of zirconium was attributed to the formation of ZrOF₂ and ZrF₄ [3, 5]. Ti exhibited high corrosion resistance than zirconium alloy when exposed to boiling nitric acid containing fluoride ions with ZrO(NO₃)₃ as complexing agent [3]. At the boiling condition of 11.5 M $HNO_3 + 0.05$ M NaF, the corrosion rate of Ti was reported to be ~ 3.1 mm/y [3]. For a

- P. M. Ranjith pmranjith10@gmail.com
- S. Ningshen ning@igcar.gov.in
- S. Ramanathan srinivar@iitm.ac.in
- Corrosion Science and Technology Division, Indira Gandhi Centre for Atomic Research (IGCAR), Kalpakkam 603102, India
- Department of Chemical Engineering, Indian Institute of Technology-Madras, Chennai 600036, India



[☑] J. Jayaraj jrajb4u@gmail.com; jraj@igcar.gov.in

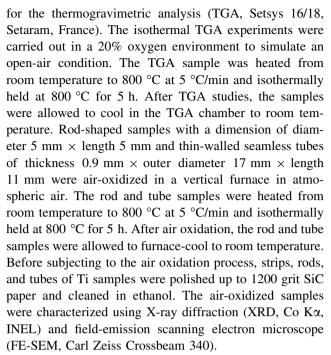
thermosiphon-type Ti electrolytic dissolver vessel shown elsewhere [6], one of the critical parts is the Ti thermowell tube due to its very small wall thickness of about 0.9 mm. Under the corrosive conditions, the estimated life of such Ti thermowell tube is about ~ 0.29 year, which is very small and unacceptable when compared to the life expectancy of a spent nuclear reprocessing plant. The polarization studies of Ti in 4.5 M H₂SO₄ + 0.25 M NaF clearly showed the active and passive regions [7]. The anodic dissolution of Ti was studied by electrochemical impedance spectroscopy (EIS) technique in 1.0 M HClO₄ with varying concentration of NaF from 0.001 to 0.1 M. At a NaF concentration > 0.001 M, dissolution of Ti was significant involving adsorbed intermediate species [8]. The dissolution of Ti in 1 M Na₂SO₄ + 0.1 M HF was modeled with a four-step reaction mechanism involving Ti³⁺ and Ti4+ intermediate species [9]. All these studies confirmed that the presence of fluoride ion enhanced the dissolution of titanium.

To improve the corrosion and tribo-corrosion resistance of titanium and its alloys, several surface modification methods have been explored. Surface modification techniques such as chemical [10–12], electrochemical [13], sol-gel [14, 15], chemical vapor deposition [16], physical vapor deposition [17], plasma spray [18], ion implantation [19, 20], and air oxidation [21, 22] have been employed. Surface modification by air oxidation has been proposed to improve the corrosion resistance of Ti in the vapor phase of boiling nitric acid [23]. Also, argon-shrouded plasmasprayed tantalum coating has been developed as an overlay to improve the corrosion behavior of the Ti in nitric acid containing fluoride ions [24]. When compared to other surface modification techniques, air oxidation of Ti in a furnace at high temperatures is the simplest method to generate a protective TiO₂ barrier layer.

Thus, in this work, to understand the electrochemical behavior, linear polarization and electrochemical impedance studies of the air-oxidized Ti were investigated and compared with the results of un-oxidized Ti, i.e., bare Ti. The electrochemical studies were carried out in nitric acid and nitric acid containing fluoride ions at room temperature. Further, the corrosion studies of air-oxidized Ti thermowells were evaluated in boiling nitric acid containing fluoride ions and compared with that of bare Ti thermowells.

2 Materials and Methods

Commercially pure titanium (Ti, grade 2) was used for evaluating the air oxidation behavior and its corrosion resistance in fluorinated nitric acid. Strip-shaped specimens of size $10 \text{ mm} \times 10 \text{ mm} \times 1.5 \text{ mm}$ were made from Ti



The electrochemical experiments were performed with rod-shaped Ti and air-oxidized Ti working electrodes of diameter 5 mm × length 5 mm. The working electrodes were mounted into Teflon rods with only one face of the electrodes exposed to the electrolyte. The rotating disk electrode (Pine Instruments) setup was used to control the working electrode speed at 900 rpm. A platinum wire and Ag/AgCl (3.5 M KCl) were used as the counter and reference electrodes, respectively. The PARSTAT 2263 (Princeton Applied Research) potentiostat was used to conduct the electrochemical experiments. The electrolyte used was 11.5 M HNO₃ and 11.5 M HNO₃ + 0.05 M NaF at room temperature. Before each experiment, the working electrodes were rinsed and ultrasonicated with ethanol.

The initial open-circuit potential (OCP) was measured, and it was observed that the stable OCP was achieved within 15 min. The electrochemical experiments were performed after the stabilization of OCP. The linear polarization curve was obtained in a potential range of \pm 10 mV versus OCP, at a scan rate of 0.5 mV/s. Stern-Geary equation [25] could be used to estimate the polarization resistance (R_P) by Eq. 1.

$$R_{\rm P} = \frac{1}{i_{\rm corr}} (E - E_{\rm corr}) \tag{1}$$

where E is the potential, $E_{\rm corr}$ is the corrosion potential, and $i_{\rm corr}$ is the corrosion current density. The electrochemical impedance spectroscopy (EIS) data were obtained by applying an AC perturbation of 20 mV on the working electrode held at OCP. A frequency range (100 kHz–10 mHz) with seven frequencies per decade (logarithmically spaced) was applied. Tafel extrapolation technique



assumes that the electrode is not passivated at anodic potentials, whereas Ti passivates in nitric acid under anodic conditions [9]. In case of air-oxidized Ti, active dissolution is not expected even at OCP. Since the assumptions employed in the Tafel extrapolation are not satisfied, potentiodynamic polarization and Tafel extrapolation are not used to estimate the corrosion rate in this work. The polarization resistance (R_P) measured from linear polarization data under rotating (900 rpm) and non-rotating conditions were used to study the effect of hydrodynamics on dissolution. The impedance experiments were conducted only at rotating conditions to eliminate the mass transfer limitations in the electrolyte. The R_P value of the air-oxidized Ti sample obtained from linear polarization and electrochemical impedance was compared with that of the un-oxidized Ti, i.e., bare Ti.

The weight loss experiments were performed for both Ti and air-oxidized Ti tubes in 11.5 M HNO₃ + 0.05 M NaF solution at room (25 °C) and boiling (120 °C) temperatures. By following the ASTM A262 Practice C procedure [26], the tube samples were exposed for a period of 48 h in boiling 11.5 M HNO₃ + 0.05 M NaF solution, and the vapors produced were refluxed using a cold finger setup. After each test period of 48 h, the tube samples were removed, cleaned with distilled water, and air-dried, and the change in weight was measured in a microbalance. After every 48 h, the fresh electrolyte was used, and the samples were exposed for a total exposure period of 240 h. The corrosion rates from weight loss measurements were calculated using Eq. 2.

Corrosion rate =
$$\frac{8.76 \times 10^4 \times W}{\rho \times A \times t}$$
 (2)

where the corrosion rate is expressed in mm/y, W is weight loss in g, ρ is the density of the sample (Ti: 4.5 g cm⁻³, TiO₂: 4.23 g cm⁻³), A is the exposed surface area in cm², and t is exposed time in h. It is worth mentioning that for the electrochemical and weight loss studies, in case of the oxidized sample, no further polishing was carried out, i.e., as-oxidized condition was used, and for the bare Ti samples polishing up to 1200 grit SiC paper was maintained.

3 Results and Discussion

3.1 Characterization of Air-Oxidized Ti

The mass gain data obtained by the thermogravimetric study of Ti at 800 °C for 5 h is shown in Fig. 1. During the isothermal study, the power law (Eq. 3) is used to describe the mass gain behavior of Ti

$$\Delta m = k t^n \tag{3}$$

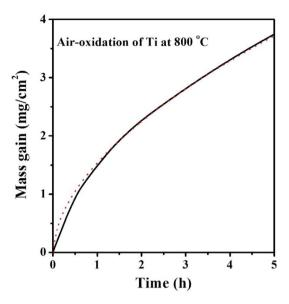


Fig. 1 Isothermal TGA behavior of Ti at 800 °C for 5 h in a 20% oxygen environment to simulate an open-air condition. Experimental results are shown as continuous lines, and the best-fitted line is shown as a dotted line

where Δm is the mass gain/total surface area (mg cm⁻²), k is the rate constant (mg cm $^{-2}$ h $^{-1}$), t is isothermal holding time (h), and n is the exponent value for t. The best-fitted power law curve is plotted as a dotted line (Fig. 1), and the fitted k and n values are 1.54 mg cm⁻² h⁻¹ and 0.55, respectively. It is seen that the model fit is very good and only slight deviations are observed in the initial stage. The n value is close to 0.5, representing a near-parabolic growth law. The pioneering work of Kofstad et al. has described the effect of oxidation temperature on the rate laws of oxide growth on the titanium [27]. It has been identified that if the oxidation temperature > 1000 °C, the mass gain obeys the linear law and results in spallation of the un-protective thick TiO₂ layer. On the other hand, if the oxidation temperature is in the range of 600–850 °C, the mass gain obeys parabolic rate law and results in the formation of protective rutile TiO₂. Due to the parabolic growth, a protective and intact oxide layer of a thickness of about 35 µm as shown in Fig. 2a is observed. The formations of the dense and faceted morphology of the rutile TiO2 phase is observed in SEM (Fig. 2b) and is confirmed by XRD analysis (JCPDF PDF#898304) (Fig. 2c). The oxidized rod and thin tube samples also exhibit similar rutile pattern and morphology.

3.2 Linear Polarization Behavior of Ti and Air-Oxidized Ti

The linear polarization curves for the bare Ti in nitric acid (Fig. 3a) and nitric acid containing fluoride ions (Fig. 3b)



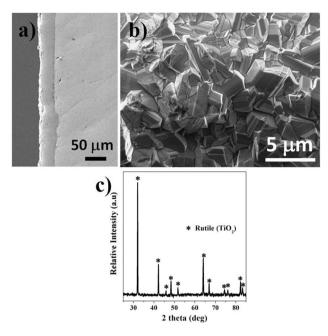


Fig. 2 SEM micrograph of air-oxidized Ti a cross section b surface morphology, and c XRD results of air-oxidized Ti

at room temperature have been recorded at both rotating and non-rotating conditions. Figure 3a, b show the linear relationship between the current density and potential for Ti in both the test solutions. The $R_{\rm P}$ values estimated from the reciprocal of the slopes of the linear polarization curves (Fig. 3a, b) are given in Table 1. When compared to $R_{\rm P}$ value in the nitric acid environment, the value obtained in nitric acid containing fluoride ions is about 150 times smaller with rotation and about 45 times smaller without rotation. The large $R_{\rm P}$ values obtained for Ti in nitric acid ($\sim 4.4 \times 10^3~\Omega~{\rm cm}^2$) indicate the high corrosion resistance of Ti which is attributed to the formation of a thin passive film of TiO₂ as shown in Eq. 4 [28, 29].

$$3Ti + 4HNO_3 \leftrightarrow 3TiO_2 + 4NO + 2H_2O; \Delta G_r^0/kJ \, mol^{-1}$$

$$= -846$$
(4)

where ΔG_r^0 is the standard Gibbs free energy change for the reaction (r) and it is calculated using the standard free energy values [30] for the products and reactants of the reaction under standard conditions. The negative sign indicates that the reaction proceeds spontaneously, and the highest value is the most favorable one. For the Ti in nitric acid, the obtained $E_{\rm corr}$ ($\sim 900 \, {\rm mV}$) and $R_{\rm P}$ values are similar under rotating and non-rotating conditions, which indicates that the passive film formation is not significantly affected by the hydrodynamic effect. As the dissolution of Ti in nitric acid is very low, the process will be reactioncontrolled, not mass transfer-controlled and will not be affected by the rotation of the electrode. The lower R_P value of Ti in nitric acid containing fluoride ions compared to non-fluorinated nitric acid indicates that the TiO₂ film is unstable and its breakdown results in the dissolution of Ti in nitric acid containing fluoride ions as shown in Eqs. 5 and 6 [3].

$$Ti + 2NaF + 2HNO_3 \leftrightarrow TiO_2 + 2NaNO_2 + 2HF; \Delta G_r^0/kJ \, mol^{-1} = -787$$
 (5)

$$Ti + 6NaF + 6HNO_3 \leftrightarrow TiF_4 + 4NaNO_3 + 2NaNO_2 + 2HF; \Delta G_r^0/kJ mol^{-1} = -915$$
 (6)

The $R_{\rm P}$ value of Ti in nitric acid containing fluoride ions with the rotation of the electrode (27.9 Ω cm²) has been found to be three times smaller than that without rotation (94.7 Ω cm²). This indicates that the dissolution is enhanced with the rotation of the electrode. The Ti is expected to form TiF₄ while reacting with nitric acid containing fluoride ions and goes into the solution more likely in the form of TiF_6^{2-} ions [3, 8, 31]. Under non-



Material	Environment	E _{corr} mV versus Ag/Ag	gCl	$R_{\rm P} \Omega.{ m cm}^2$		
		Without rotation	With rotation (900 rpm)	Without rotation	With rotation (900 rpm)	
Ti	11.5 M HNO ₃	889	900	4319.33	4414.92	
				(0.53%)	(0.81%)	
	$11.5 \text{ M HNO}_3 + 0.05 \text{ M NaF}$	373	315	94.70	27.9	
				(0.89%)	(1.68%)	
Air-oxidized Ti	11.5 M HNO ₃	161	156	9.10×10^4	7.26×10^4	
(Rutile TiO ₂)				(0. 85%)	(0.87%)	
	$11.5 \text{ M HNO}_3 + 0.05 \text{ M NaF}$	137	138	5.07×10^4	5.20×10^4	
				(0.55%)	(0.46%)	

Table 1 Linear polarization parameters of Ti and air-oxidized Ti (rutile TiO_2) obtained in 11.5 M HNO₃ and 11.5 M HNO₃ + 0.05 M NaF at room temperature

rotating conditions, the corroded products on the surface can hinder the mass transfer of fresh nitric acid containing fluoride ions on to the surface of the metal electrode and thereby reduce the dissolution of Ti. With the rotation of electrode, the TiF₄ may quickly move into the bulk of the solution, and a uniform concentration of nitric acid containing fluoride ions can be maintained on the surface of the electrode, and thereby increase the dissolution rate.

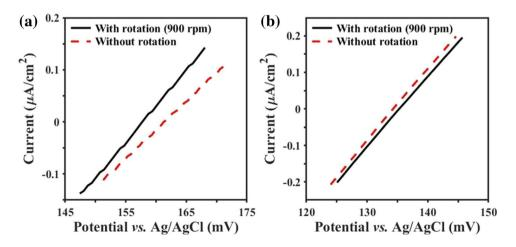
The linear polarization curves for the air-oxidized Ti (Rutile TiO_2) in nitric acid (Fig. 4a) and nitric acid containing fluoride ions (Fig. 4b) are recorded at room temperature with and without rotation, and the obtained R_P values are shown in Table 1. There is no significant difference in R_P values of air-oxidized Ti in nitric acid ($\sim 8 \times 10^4 \ \Omega \ cm^2$) under rotating and non-rotating conditions. The addition of fluoride in nitric acid slightly reduces the R_P value of air-oxidized Ti ($\sim 5 \times 10^4 \ \Omega \ cm^2$). This is probably due to the attack of fluoride ions through the thick rutile TiO_2 oxide layer. Under the rotating condition, the R_P value of air-oxidized Ti in nitric acid and nitric acid containing fluoride ions is about 16 and

1863 times higher than that of bare Ti, respectively. The several order increase in $R_{\rm P}$ value of air-oxidized Ti in nitric acid containing fluoride ions points to the significant corrosion protection offered by the air-oxidized rutile ${\rm TiO_2}$ on the surface of Ti.

3.3 Electrochemical Impedance Analysis of Ti and Air-Oxidized Ti

The electrochemical impedance spectra of bare Ti rotating at 900 rpm have been recorded at the corresponding OCP values in nitric acid and nitric acid containing fluoride ions, and the respective results are shown in Nyquist plots (Figs. 5a and 6a). The experimental data are shown as markers, while the EEC model results, described below, are shown in dashed lines. For the EEC modeling, Zsimpwin® software (Princeton Applied Research, USA) has been used. The results of linear polarization experiments show that, under stationary conditions, mass transfer of active species in the electrolyte limits the net reaction rate. When mass transfer in solution is coupled with reaction on Ti and

Fig. 4 Linear polarization behavior of air-oxidized Ti at room temperature in **a** 11.5 M HNO₃ and **b** 11.5 M HNO₃ + 0.05 M NaF at a scan rate of 0.5 mV/s





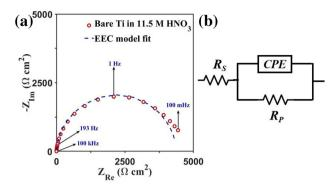


Fig. 5 Electrochemical impedance behavior of bare Ti (with a rotational speed of 900 rpm) held at OCP in 11.5 M HNO₃ at room temperature **a** Nyquist plot and **b** EEC used to model the data

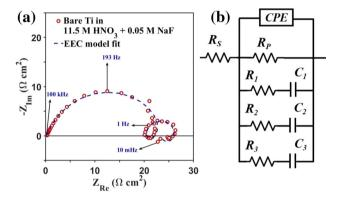
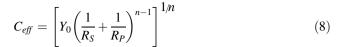


Fig. 6 Electrochemical impedance behavior of bare Ti (with a rotational speed of 900 rpm) held at OCP in 11.5 M HNO $_3+0.05$ M NaF at room temperature **a** Nyquist plot and **b** EEC used to model the data

possible mass transfer in the film in case of air-oxidized Ti, the analysis becomes very challenging. Hence, EIS experiments are performed only under rotating conditions so that the results can be analyzed assuming rapid mass transfer in the electrolyte. In nitric acid, the impedance spectra of Ti (Fig. 5a) show only one capacitance loop in the frequency range studied. The capacitance loop is a depressed semicircle and has been analyzed using an equivalent circuit of $R_{\rm S}(QR_{\rm P})$, as shown in Fig. 5b. Here, $R_{\rm S}$ is the solution resistance, Q is the constant phase element (CPE), and $R_{\rm P}$ is the polarization resistance. Q has been used in the present investigation to obtain a better fit for the experimental data [32, 33]. The impedance of Q is given in Eq. 7.

$$Z_{\mathcal{Q}} = Y_0^{-1} (j\omega)^{-n} \tag{7}$$

where Y_0 is a constant $(\Omega^{-1}s^n)$, n is the power index value of Q, ω is the angular frequency, and j is the imaginary number equal to $\sqrt{-1}$. The effective capacitance $(C_{\rm eff})$ is determined using Brug's formula [32] (Eq. 8).



The estimated C_{eff} is given in Table 2. The thickness (*d*) of the passive film that forms on Ti in nitric acid has been calculated using Eq. 9 [34].

$$d = \frac{\varepsilon \varepsilon_o}{C_{\text{eff}}} \tag{9}$$

where ε is the dielectric constant of the passive film (ε for TiO₂ is 25) and $\varepsilon_o = 8.854 \times 10^{-14}$ F cm⁻¹ is the permittivity of free space charge. The calculated thickness of the passive film formed on Ti at the OCP condition in nitric acid is much lower (~ 0.9 nm) compared to that of the oxide layer formed due to air oxidation. The R_P values are estimated based on the condition given in Eq. 10.

$$R_P = \lim_{\omega \to 0} Z_F \tag{10}$$

where Z_F is the faradaic impedance. The estimated R_P value, from EEC fit, of Ti in nitric acid is given in Table 2. A comparison of Table 1 and 2 shows that R_P estimated from LP and EIS shows a good match. The very high R_P value ($\sim 4.4 \times 10^3 \ \Omega \ cm^2$) indicates that the passive film formed on Ti is highly protective in nitric acid even if it is very thin.

The impedance spectrum obtained for Ti in nitric acid containing fluoride ions (Fig. 6a) shows a high-frequency capacitive loop, an inductive loop, and a capacitive loop at mid frequencies and another inductive loop at the low frequencies. The double layer that is formed at the interface of electrode surface and electrolyte, in parallel with the $R_{\rm P}$, is responsible for the measured capacity loop at the higher frequencies. The observed inductive loops can be treated as inductance or negative capacitance [35, 36]. The inductance arises from the electrochemical reactions with formation of intermediate adsorbed species and their relaxation [37, 38]. An equivalent circuit with three adsorbed intermediates has been used for the analysis of EIS data (Fig. 6b). While fitting the impedance data, C_1R_1 and C_2R_2 of Fig. 6b are allowed to hold negative values to represent the inductance. Previously, the dissolution of Ta, Nb, Zr, and Ti in HF has been observed and modeled with inductive loops of EIS data [9, 39–41]. The two inductance loops and the mid-frequency capacitance loop obtained (Fig. 6b) can be ascribed to the relaxation of adsorbed intermediate species. The best-fit EEC parameters are listed in Table 3. It is challenging to obtain physical insights for the Maxwell elements, and since the focus is on corrosion resistance, only R_P values have been used for further analysis. A comparison of Table 1 and Table 3 shows that $R_{\rm P}$ values of Ti in nitric acid containing fluoride ions



Table 2 Best-fit EEC parameters for Ti (with a rotational speed of 900 rpm) held at OCP in 11.5 M HNO₃ at room temperature

OCP	$R_{ m S}$	Y_0	n	$C_{ m eff}$	$R_{ m P}$
mV vs Ag/AgCl	$\Omega \text{ cm}^2$	$\Omega^{-1}~cm^{-2}~S^n$	-	$\mu F \text{ cm}^{-2}$	$\Omega \text{ cm}^2$
900	0.35	3.92×10^{-5}	0.96	24.58	4407
	(2%)	(2%)	(< 1%)		(2%)

Table 3 Best-fit EEC parameters for Ti (with a rotational speed of 900 rpm) held at OCP in 11.5 M HNO₃ +0.05 M NaF at room temperature

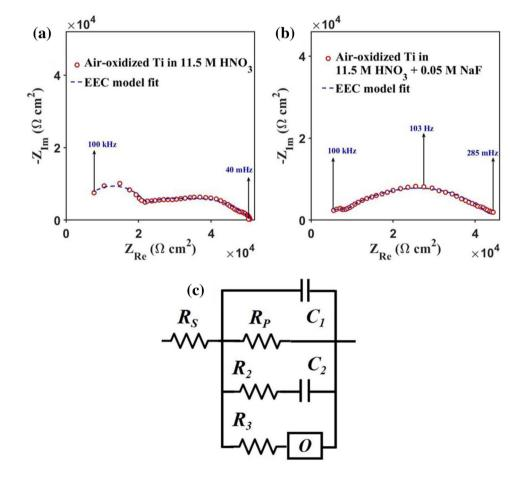
ОСР	R_{S}	Y_0	n	C_1	R_1	C_2	R_2	C ₃	R_3	$C_{ m eff}$	R_{P}
mV vs Ag/AgCl	$\Omega \ cm^2$	$\Omega^{-1}~cm^{-2}~S^n$	_	${\rm mF~cm^{-2}}$	$\Omega \ cm^2$	${\rm mF~cm^{-2}}$	$\Omega \ cm^2$	${\rm mF~cm^{-2}}$	$\Omega \ cm^2$	$\mu F \text{ cm}^{-2}$	$\Omega \text{ cm}^2$
315	0.26	1.65×10^{-4}	0.78	6.37	78.34	-0.14	-97.64	-26.33	- 164.60	9.65	23.34
	(3%)	(6%)	(< 1%)	(29%)	(12%)	(21%)	(10%)	(39%)	(25%)		(2%)

estimated from EIS and LP match well. While the R_P value of Ti in nitric acid is high, it decreases dramatically with the addition of NaF. A similar trend is also observed in R_P values obtained from LP.

The impedance spectra obtained for air-oxidized Ti rotating at 900 rpm in nitric acid and nitric acid containing fluoride ions are shown in Fig. 7a and Fig. 7b, respectively.

The experimental data and EEC model results are shown as markers and dotted line, respectively. Here, it is assumed that the diffusion of ionic species through the air-oxidized layer influences the impedance of air-oxidized Ti under rotating condition. Analyses using simpler circuits result in poor fit to the experimental data and hence have not been pursued further. In nitric acid, the impedance spectra of air-

Fig. 7 Electrochemical impedance behavior of airoxidized Ti (with a rotational speed of 900 rpm) held at OCP in **a** 11.5 M HNO₃ **b** 11.5 M HNO₃ + 0.05 M NaF at room temperature and **c** EEC used to model the data





oxidized Ti (Fig. 7a) show two different capacitance loops, one in the high and the other in low-frequency range, respectively. The capacity loop observed at the high frequency corresponds to the double layer that is formed at the interface of electrode surface and electrolyte, in parallel with the $R_{\rm P}$. The capacitance loop with depressed semicircle has been analyzed using an equivalent circuit of $R_{\rm S}(C_1R_{\rm P})$, as shown in Fig. 7c. Conversely, the low-frequency loop is modeled with a parallel combination of C_2R_2 and OR_3 . The element "O" represents the finitelength linear diffusion with the transmissive boundary condition, also known as bounded Warburg element, and the impedance ($Z_{\rm BW}$) for this diffusion is given in Eq. 11 [35, 36].

$$Z_{\rm BW} = \frac{\sigma}{\sqrt{\omega}} \tanh\left(\sqrt{\frac{j\omega}{D}}l\right) (1-j) = \frac{\sigma}{\sqrt{j\omega}} \tanh\left(\sqrt{\frac{j\omega}{D}}l\right) \tag{11}$$

where D is the diffusivity of reacting species, l is the thickness of the air-oxidized layer, and σ is the mass transfer coefficient. A similar circuit with an inductor-based Maxwell element has been used earlier to model the hydrogen oxidation in fuel cell [42]. The parameters estimated from EEC model are listed in Table 4. The parameters Y_0 and B corresponds to the Maxwell element O, and Eq. 11 can be rewritten as

$$Z_{\rm BW} = \frac{1}{Y_0 \sqrt{j\omega}} \tanh\left(B\sqrt{j\omega}\right) \tag{12}$$

The diffusivity of reacting species through the air-oxidized layer is determined from the finite-length reflective impedance parameter B as shown in Eq. 13.

$$D = \left(\frac{l}{B}\right)^2 \tag{13}$$

The impedance spectrum of air-oxidized Ti in nitric acid containing fluoride ions shows a very small capacitive loop at high frequency and another loop at a low frequency similar to Ti. The impedance spectra are modeled with the circuit shown in Fig. 7c. The corresponding estimated EEC parameters are listed in Table 4. The R_P values estimated form LP and EIS are in the same range of a few $10^4 \Omega \text{ cm}^2$ for air-oxidized Ti in both nitric acid and fluorinated nitric acid. This indicates that the oxide layer formed as a result of air oxidation at 800 °C is highly protective. For the air-oxidized Ti electrode immersed in nitric acid, the estimated diffusivity of reacting species through the film is obtained to be very low (of the order of 10^{-16} cm² s⁻¹). On the other hand, when the same electrode is immersed in fluorinated nitric acid, the estimated diffusivity in the film is relatively higher of the order of 10^{-6} cm² s⁻¹ (Table 4). It is likely that the oxide layer is attacked by the nitric acid containing fluoride ions (Eq. 14) [3], and the increas in defects may have caused an increase in the estimated diffusivity value.

$$TiO_2 + 4NaF + 4HNO_3 \leftrightarrow TiF_4 + 4NaNO_3 + 2H_2O; \Delta G_r^0/kJ \, mol^{-1} = -128$$
 (14)

3.4 Weight Loss Measurements in Nitric Acid Containing Fluoride Ions

The corrosion rates of Ti and air-oxidized Ti in nitric acid containing fluoride ions under room temperature and boiling conditions are shown in Table 5. In the given test solution, the corrosion rate of Ti under room temperature has been determined to be 0.15 mm/y, but it increases to more than 23 times under boiling condition. The as-polished Ti exhibits a metallic luster as shown in Fig. 8a. The thickness of Ti tubes get considerably reduced (Fig. 8b) when exposed in boiling fluorinated nitric acid for 48 h. The dissolution behavior of the bare Ti, when exposed to boiling fluorinated nitric acid, is likely due to the formation of TiF₄, as shown in Eq. 6.

Table 4 Best-fit EEC parameters for air-oxidized Ti (with a rotational speed of 900 rpm) held at OCP in 11.5 M HNO₃ and 11.5 M HNO₃. + 0.05 M NaF at room temperature

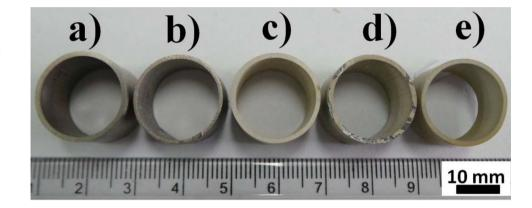
Solution	OCP mV vs Ag/ AgCl	$R_{\rm S} + R_{\rm film}$ $\Omega \ { m cm}^2$	C ₁ F cm ⁻²	C ₂ F cm ⁻²	R_2 $\Omega \text{ cm}^2$	$\begin{array}{c} O - Y_0 \\ \Omega^{-1} \text{ s}^{1/2} \end{array}$	O-B	R_3 $\Omega \text{ cm}^2$	$R_{\rm P}$ $\Omega \ {\rm cm}^2$	$\frac{D}{\text{cm}^2} \text{ s}^{-1}$
11.5 M HNO ₃	143	3.39×10^3 (12%)	1.38×10^{-10} (5%)	3.98×10^{-10} (39%)	1.25×10^5 (28%)	4.29×10^{-7} (7%)	1.14×10^5 (7%)	3.89×10^4 (11%)	4.78×10^4 (1%)	9.43×10^{-16}
$11.5~\mathrm{M} \\ \mathrm{HNO_3} + 0.05~\mathrm{M} \\ \mathrm{NaF}$	138	3.84×10^3 (4%)	3.96×10^{-10} (8%)	3.81×10^{-10} (26%)	2.83×10^4 (24%)	7.96×10^{-7} (2%)	1.89 (10%)	6.13×10^3 (10%)	4.13 × 10 ⁴ (< 1%)	3.43×10^{-6}



	ated from weight loss experiments	.5 M 1111O ₃ + 0.05 M 11al at 100111 ten	iperature (23°C) and borning
Material conditions	Corrosion testing temperature (°C)	Corrosion testing period (h)	Corrosion rate (mm/y)

Material conditions	Corrosion testing temperature (°C)	Corrosion testing period (h)	Corrosion rate (mm/y)
Bare Ti tube	25	240	0.15 ± 0.03
	120	48	3.5 ± 0.12
Air-oxidized Ti tube	25	240	negligible
	120	48	0.003 ± 0.001
	120	240	0.025 ± 0.01

Fig. 8 Images of Ti tubes before and after exposure to boiling 11.5 M HNO₃ + 0.05 M NaF, **a–b** bare Ti; **a** before exposure; **b** exposed for 48 h; and, **c–e** airoxidized Ti; **c** before exposure; **d** exposed for 240 h; and, **e** exposed for 48 h



In contrast, the as-prepared condition of the air-oxidized Ti exhibits a ceramic nature with pale yellow color as shown in Fig. 8c. The weight loss of air-oxidized Ti in the same test solution under room temperature for an immersion period of 240 h is observed to be negligible. In comparison with Fig. 8c, a significant attack along the ringside (Fig. 8d) is observed for the air-oxidized Ti tube when exposed to the boiling condition of the solution for 240 h. When exposed only for 48 h at the boiling condition, an un-attacked surface with slight discoloration (Fig. 8e) is observed for the air-oxidized Ti tube. As the immersion period is increased from 48 h to 240 h, the corrosion rate increases by more than eight times for the air-oxidized Ti.

The increase in dissolution rate with immersion time may occur because, after a certain period, the dissolution of air-oxidized layer will expose the underlying Ti to the boiling nitric acid containing fluoride ions (Fig. 8d). It is likely that the dissolution rate will increase monotonically with immersion time and will stabilize at a high rate once the air-oxidized TiO₂ layer dissolves completely. Until then, oxide layer will protect the underlying Ti, and the dissolution of air-oxidized Ti in boiling nitric acid containing fluoride ions for a period of 240 h is observed to be 140 times lower than that for bare Ti exposed for a shorter period of 48 h.

It is seen from Table 5 that at room temperature, in fluorinated nitric acid, the corrosion rate of air-oxidized Ti

calculated from weight loss experiments is negligible. On the other hand, comparison of R_P values estimated from LP and EIS (listed in Tables 1, 2, 3, and 4) gives a better understanding of the improvement in corrosion resistance by the air oxidation of Ti. It is challenging to conduct electrochemical experiments in boiling nitric acid and fluorinated nitric acid, whereas weight loss experiments give a better estimate of corrosion rate in boiling conditions. By combining the results of electrochemical experiments performed at room temperature and weight loss experiments performed in nitric acid containing fluoride ions at room temperature as well as boiling conditions, it is deduced that air-oxidized Ti exhibits better corrosion protection than Ti in fluorinated nitric acid.

4 Conclusion

The corrosion protection offered by air-oxidized Ti in nitric acid containing fluoride ions was investigated using electrochemical techniques at room temperature and the weight loss experiments at boiling temperature of 120 °C. The major conclusions of the present studies are summarized as follows:

(a) The EIS behavior of the Ti and air-oxidized Ti in nitric acid containing fluoride ions was successfully modeled with suitable electrochemical equivalent



circuits, and the estimated R_P values showed a good match with linear polarization. The high R_P value of the air-oxidized Ti sample indicated a high corrosion resistance than that of Ti. The diffusivity (D) of reacting species through the air-oxidized layer was determined from the finite-length reflective impedance parameter (B), and it was very well correlated with the corrosion behavior.

(b) The weight loss studies confirmed that the air-oxidized Ti showed excellent corrosion protection in boiling fluorinated nitric acid as the corrosion rate is 1166 times slower than that of Ti (3.5 mm/y).

Open Access This article is distributed under the terms of the Creative Commons Attribution 4.0 International License (http://creativecommons.org/licenses/by/4.0/), which permits unrestricted use, distribution, and reproduction in any medium, provided you give appropriate credit to the original author(s) and the source, provide a link to the Creative Commons license, and indicate if changes were made.

References

- 1. Natarajan R. Raj B. J Nucl Sci Technol 44 (2007) 393.
- Bernard C, Mouroux J P, Decours J, Demay R, Simonnet J, Zirconium-made equipment for the new La Hague reprocessing plants, Japan Atomic Industrial Forum, Japan (1991).
- Jayaraj J, Krishnaveni P, Krishna D N G, Mallika C, Mudali U K, J Nucl Mater 473 (2016) 157.
- Uriarte A L, Rainey R H, Dissolution of high-density UO2, PuO2, and UO2-PuO2 pellets in inorganic acids, Technical Report ORNL—3695, The U.S. Atomic Energy Commission, Washington (1965) p 1.
- Jayaraj J, Nanda Gopala Krishna D, Mallika C, Kamachi Mudali U, Trans Indian Inst Metals 71 (2018) 521.
- 6. Raj B, Mudali U K, Prog Nucl Energy 48 (2006) 283.
- 7. Kelly J J, Electrochimica Acta 24 (1979) 1273.
- 8. Kong D -S, Feng Y -Y, J Electrochem Soc 156 (2009) C283.
- Fasmin F, Praveen B, Ramanathan S, J Electrochem Soc 162 (2015) H604.
- 10. Lu X, Zhao Z, Leng Y, Mater Sci Eng C 27 (2007) 700.
- Yousefpour M, Afshar A, Chen J, Zhang X, Mater Design 28 (2007) 2154.
- Pattanayak D K, Kawai T, Matsushita T, Takadama H, Nakamura T, Kokubo T, J Mater Sci Mater Med 20 (2009) 2401.
- Fazel M, Salimijazi H R, Shamanian M, ACS Appl Mater Interfaces 10 (2018) 15281.
- Montenero A, Gnappi G, Ferrari F, Cesari M, Salvioli E, Mattogno L, Kaciulis S, Fini M, J Mater Sci 35 (2000) 2791.
- Kim H -W, Koh Y-H, Li L-H, Lee S, Kim H -E, Biomaterials 25 (2004) 2533.

- 16. Liu X, Chu P K, Ding C, Mater Sci Eng R Rep 47 (2004) 49.
- 17. Hee A C, Jamali S S, Bendavid A, Martin P J, Kong C, Zhao Y, Surf Coat Technol 307 (2016) 666.
- Mittal M, Natha S K, Prakash S, J Min Mater Charact Eng 10 (2011) 1041.
- Krupa D, Baszkiewicz J, Kozubowski J A, Barcz A, Sobczak J W, Biliński A, Lewandowska-Szumieł M, Rajchel B, Biomaterials 22 (2001) 2139.
- Krupa D, Baszkiewicz J, Kozubowski J A, Barcz A, Sobczak J W, Biliński A, Lewandowska-Szumieł M, Rajchel B, Biomaterials 23 (2002) 3329.
- 21. Schutz R W, Covington L C, Corrosion 37 (1981) 585.
- Kumar S, Narayanan T S N S, Ganesh Sundara Raman S, Seshadri S K, Mater Sci Eng C 30 (2010) 921.
- Shankar A R, Karthiselva N S, Mudali U K, Surf Coat Technol 235 (2013) 45.
- Vetrivendan E, Jayaraj J, Ningshen S, Mallika C, Kamachi Mudali U, J Therm Spray Technol 27 (2018) 512.
- 25. Stern M, Geary A L, J Electrochem Soc 104 (1957) 56.
- 26. Guidelines for avoiding intergranular corrosion and stress corrosion in austenitic stainless steel components of fuel reprocessing plants, Regulatory Guide 3.37, U.S. Nuclear Regulatory Commission, USA (1975) p 1.
- Kofstad P, Hauffe K, Kjollesdal H, Acta Chemica Scandinavica 12 (1958) 239.
- Jayaraj J, Thinaharan C, Ningshen S, Mallika C, Kamachi Mudali U, Intermetallics 89 (2017) 123.
- Jayaraj J, Ravi Shankar A, Kamachi Mudali U, Electrochimica Acta 85 (2012) 210.
- Knacke O, Kubaschewski O, Hesselmann K, Thermochemical Properties of Inorganic Substances, 2nd Ed, Springer, New York (1991)
- 31. Sutter E M M, Goetz-Grandmont G J, Corros Sci 30 (1990) 461.
- Brug G J, van den Eeden A L G, Sluyters-Rehbach M, Sluyters J H, J Electroanal Chem Interfacial Electrochem 176 (1984) 275.
- Brug G J, Sluyters-Rehbach M, Sluyters J H, Hemelin A, J Electroanal Chem Interfacial Electrochem 181 (1984) 245.
- Hirschorn B, Orazem M E, Tribollet B, Vivier V, Frateur I, Musiani M, Electrochimica Acta 55 (2010) 6218.
- 35. Lasia A, Electrochemical impedance spectroscopy and its applications, Springer, New York (2014).
- Orazem M E, Tribollet B, Electrochemical impedance spectroscopy, 1st ed., Wiley-Interscience, United States (2008).
- Harrington D A, van den Driessche P, J Electroanal Chem 567 (2004) 153.
- 38. Franceschetti D R, Macdonald J R, J Electroanal Chem Interfacial Electrochem 82 (1977) 271.
- Ranjith P M, Rao M T, Sapra S, Suni I I, Srinivasan R, J Electrochem Soc 165 (2018) C258.
- 40. Mandula T R, Srinivasan R, J Solid State Electrochem (2017) 1.
- Amrutha M S, Rao M T, Ramanathan S, J Electrochem Soc 165 (2018) C162.
- 42. Wagner N, Friedrich K A, Fuel Cells 9 (2009) 237.

Publisher's Note Springer Nature remains neutral with regard to jurisdictional claims in published maps and institutional affiliations.

